Comparison of Waveguide Coupled and Coaxial Coupled ECRA Magnetic Nozzle Thruster using a Thrust Balance

Simon Peterschmitt, Denis Packan

Comparison of Waveguide Coupled and Coaxial Coupled ECRA Magnetic Nozzle Thruster using a Thrust Balance

IEPC-2019-188

Presented at the 36th International Electric Propulsion Conference
University of Vienna • Vienna, Austria
September 15-20, 2019

Simon Peterschmitt[1] and Denis Packan[2]
DPHY, ONERA, Université Paris Saclay, F-91123 Palaiseau – France

Abstract: The Electron Cyclotron Resonance (ECR) thruster takes advantage of the well-known electron cyclotron resonance of the cold uniform magnetized plasma in order to efficiently ionize the propulsive gas and heat up the electrons of the plasma. Several coupling structures can be considered to transfer the incoming microwave power into the plasma. This article exposes the results of an experiment on a circular waveguide coupled thruster. In particular, thrust balance measurements are performed for the first time. A thrust of 430 µN at 1.5sccm and 16W of input power is measured resulting in 3.8% of total efficiency. Ion energy distribution and ion current density are measured. The results are compared to a coaxial coupled thruster carefully designed so that only its coupling structure differs from that of the thruster under study.

Nomenclature

ECR = Electron Cyclotron Resonance
ECRA = Electron Cyclotron Resonance Acceleration. Acronym used to refer to the ECR thruster developed at ONERA
ONERA = Office National d'Etudes et de Recherches Aérospatiales
JLU = Justus-Liebig-Universität

I. Introduction

MICRO-propulsion has been identified has one of the major technological challenges on the rapidly growing market of small satellites[1]. Miniaturization of existing technologies as well as innovative concepts have been proposed. The Electron Cyclotron Resonance Acceleration (ECRA) thruster currently under development at ONERA in the framework of the MINOTOR project[2] appears as a potentially disruptive technology on this market. This concept could lead to a robust, easy to operate, and low cost propulsion system.

The project includes experimental and simulation efforts across the MINOTOR consortium. It focuses on the thruster itself but also addresses issues at system level such has the development of a dedicated microwave generator and prospective work regarding integration on satellite. Both experimental[3,4] and PIC simulation efforts[5] are conducted at ONERA in order to move forward with the development of the thruster.

[1] PhD Student, DPHY, simon.peterschmitt@onera.fr
[2] Head of Lightning Plasma and Applications Unit, DPHY, denis.packan@onera.fr

Figure 1 is a schematic view of a typical implementation of the thruster. It consists of a 27.5 mm diameter and 20 mm long semi-open coaxial coupling structure. Xenon gas is injected at a typical mass flow of 1sccm. Typically, 25 W of microwave power at 2.45 GHz are fed through a boron nitride "backplate" at the close end of the coaxial structure. It is immersed in a static and divergent magnetic field that is created by an annular permanent magnet.

The all the necessary power for ionization of the gas and heating of the electrons is provided by the absorption of the microwave. Hot electrons expend in the magnetic nozzle creating the accelerating potential for the ions.

One of the difficulties to further development of the thruster is the study of the erosion of the inner conductor of the coaxial coupling structure and associated material deposition, in particular on the "backplate". Waveguide coupling of the input microwave power to the plasma appears has a possible way to circumvent this issue since no inner conductor is required in this case.

Waveguide coupling for ECR thrusters has been studied in the past although the measured performances were quite poor. Studies started in the 1960s with Gibbons and Miller[6]. They demonstrated the thrust producing ability of the design, reported 80-90% coupling from the microwave energy to the plasma and 1% total efficiency. The plasma was created in a rectangular RG-48/U waveguide (72x34mm) using 320W input power at 2.45GHz. A more detailed investigation was conducted in the framework of the CYLCOPS study[7] as well as in Crimi's doctoral work[8]. Several designs were tested to explore the effect of injection, microwave frequency, input power, geometry but no configuration seemed to stand out. Later, in the 1990s, Sercel[9] investigated the optimization of a plasma thruster using a circular waveguide of 128 mm in diameter, with typically 700 W input power at 2.1GHz. A similar level of coupling and 2 % total efficiency were reported.

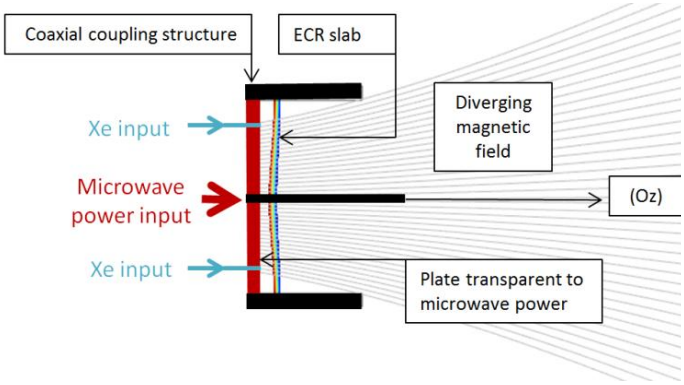

Figure 1. Schematic of a typical implementation of the coaxial ECR thruster

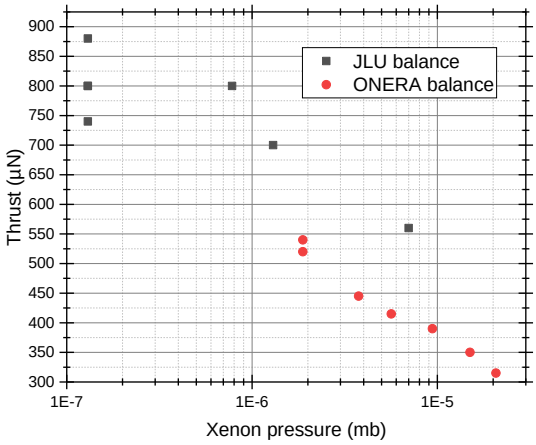

Figure 2. Thrust as a function of pressure with JLU balance at Jumbo facility and with ONERA balance at B61 facility. The

Notwithstanding these previous results, with the expertise acquired at ONERA on the coaxial ECRA thruster, it seems relevant to investigate again the waveguide coupled ECR thruster for at least three reasons. (i) In previous studies, no direct thrust measurement was performed. Yet it is well known, in particular on this thruster, that the estimation of thrust from probe measurement can bear very significant discrepancy with respect to direct thrust measurement (see below the section II.C.3). (ii) A critical lack of accuracy of several key measurements including the input microwave power and the input gas mass flow rate blurs the assessment of the performances. (iii) It was shown repeatedly that a high background pressure in the test facility is a critical parameter decreasing the ECRA thruster performances[10]. Figure 2 shows the results from a test campaign conducted at ONERA and JLU, thus comparing the thruster performance on two facilities, with a separate gas input varying the background pressure. The decrease of thrust with background Xe pressure for a given set point of the thruster is very clear, even below 10^{-6} mbar. The offset between the two sets of data could be attributed to facility effect. It could for example be a consequence of gap in diameter of the tank. The JLU Jumbo facility is 3m in diameter whereas the ONERA B61 is 1m in diameter.

This paper presents some of the results of an experimental investigation of waveguide coupled ECR thruster. Section II exposes the design of the waveguide thruster, describes the test set up and presents some key features of the coaxial ECRA thruster in order to put into perspective the experimental results on the waveguide thruster presented in section III. Section IV is the conclusion.

II. Presentation of the thruster and experimental set-up

A. The thruster design

The thruster tested consists of a 27.5 mm diameter and 20 mm long waveguide coupling structure. Behind is a filled coaxial to waveguide transition assembled to a permanent magnet. A material with high dielectric constant is required in order for the 2.45GHz microwave to be propagating in a structure of such diameter.

The inserted ceramics material has been measured using a dedicated test set-up to have a relative permittivity $\boldsymbol{\epsilon = 8.7 - 0.07j}$ at the working temperature of the thruster which is around 110°C. Given the appreciable heat production implied by the imaginary part of the permittivity, it is necessary to allow heat dissipation. A tight fastening of the dielectric material ensures appropriate thermal contact with the rest of the mechanical structure. This tight fastening is obtained with shrink-fitting of the ceramics cylinder into the surrounding part.

The microwave power is fed through a rigid coaxial line. Careful microwave design enables transmission up to the back end of the plasma volume without reflection.

Xenon gas is collected in a plenum from the gas feed tube and injected through six injection holes distributed radially at the back end of the plasma volume. Gaskets ensure gas tightness.

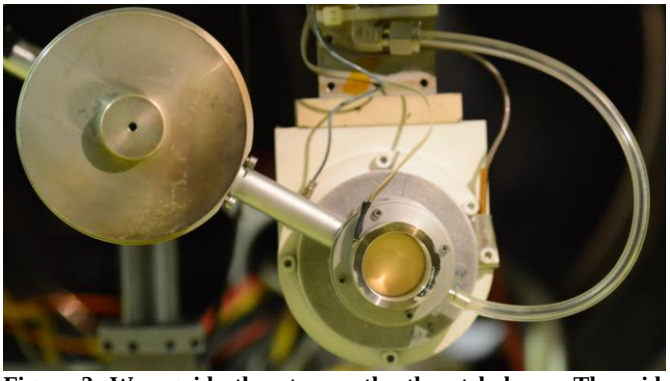

Figure 3. Waveguide thruster on the thrust balance. The wide cylinder on the left is a coaxial to waveguide transition designed for testing on the thrust balance. It enables microwave feeding without mechanical coupling of the balance arm

B. Description of the test set-up

Figure 3 is a picture of the thruster mounted on the thrust balance and equipped with a coaxial to waveguide transition. A pair of coaxial to waveguide transitions facing each other and separated by a 2 mm gap achieve excellent transmission of the microwave power without any mechanical contact. One is placed on the balance pendulum arm and the other is stationary. Therefore microwave power transmission and free movement of the balance arm are achieved simultaneously[11]. The balance pendulum arm is held into vertical position by a PID controller. The sensor of the PID loop is a capacitive sensor and the actuator is a coil acting on magnets placed on the pendulum arm. Before each test, a calibration procedure determines the relation between the output voltage of the PID and the force exerted on the arm of the balance. This relation is proportional.

Figure 4. Probes mounted on a rotation stage. Left: guard ring Faraday for the measurement of ion current. Right: gridded Faraday for the measurement of most probable ion energy.

Two electrostatic probes are mounted on a rotation stage at 26.5 cm from the exit plane of the thruster (Figure 4). The gridded Faraday probe is a simplified retarding potential analyzer (RPA) consisting of a collector biased at a chosen potential preceded by a grid at a floating potential. This grid is screening the collector voltage thus preventing a sheath expansion outside the probe. Otherwise, the probe would draw a diverging electron current when the collector voltage is swept to highly positive values. Since the longitudinal energy distribution of electrons is well separated from that of the ions, this simple device is able to provide an estimate of the ion energy distribution function around the most probable ion energy. A commercial Hiden mass spectrometer and ion analyzer is also used. It provides a more complete and accurate measurement of the ion energy distribution function, however only at a fixed angle: on the axis of symmetry of the thruster.

The gridded Faraday is able to measure an ion current density. However, because of uncertainties related to the grid (mainly transparency and secondary emission) a Faraday probe with guard ring is preferred to measure ion current density. The collected current is read while the collector and the guard ring are held at the same negative potential of typically -200V in order to repel all electrons and collect ion. The presence of the guard ring ensures flat

equipotential surfaces in front of the probe in order to avoid collection of ion current on an effective surface wider than the collector surface. The guard ring is 5cm in diameter.

The thruster is equipped with temperature probes and a measurement of its potential.

Experiments are performed in the B61 facility at ONERA. It is a 4m long and 1m in diameter tank with a pumping speed for Xe around 8000 L/s. The base pressure is around 8.10^{-7} mbar.

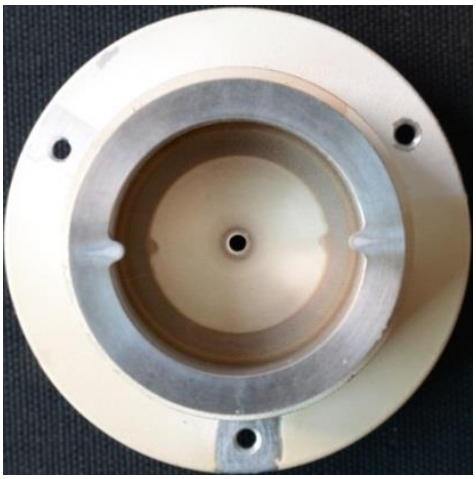

Figure 5. Deposition on the boron nitride "backplate" in the shadow of the front section of the thruster structure

C. Typical features of the thruster

1. Oscillating movement of electrons

Figure 5 is a picture of a thruster that was run for several hours. The white central part of the "backplate" looks as it was before performing the test whereas some material seems to be deposited in the peripheral area. The deposit exhibits metallic reflections. It was proved to come from the antenna by electron X-ray fluorescence. A reasonable explanation for this observation is the following. While the thruster is running, material from the walls is uniformly deposited on the "backplate". This deposit is simultaneously eroded by the plasma but only in the central region where dense plasma is present. Measurement of the radius of this central cylinder shows that it is a section of the magnetic "tube" that go through the exit section of the thruster. This magnetic tube is sketched on Figure 1. The fortunate presence of two ergots on the exit section and their associated "shadows" contribute to support this interpretation.

This observation substantiate the claim made in[13] that the plasma can be modeled as strongly confined by the magnetic field and that there exists an oscillating movement of electrons along magnetic field lines extending well outside the physical structure of the thruster. This oscillating movement of the guiding center of electrons can be described by the equation of motion

$$m\frac{dv_z}{dt} = -\mu\frac{\partial B_z}{\partial z} + e\frac{\partial \phi}{\partial z}$$

where m is the electron mass, $\mu = mv_\perp^2/(2B)$ is the magnetic moment, e is the absolute value of the elementary charge and ϕ the electrostatic potential. Electrons created in the thruster oscillate in the well of effective potential energy $U_{eff} = \mu B - e\phi$. They are confined on the thruster side (left) by the converging magnetic field and on the plume side (right) by the electrostatic potential Figure 6).

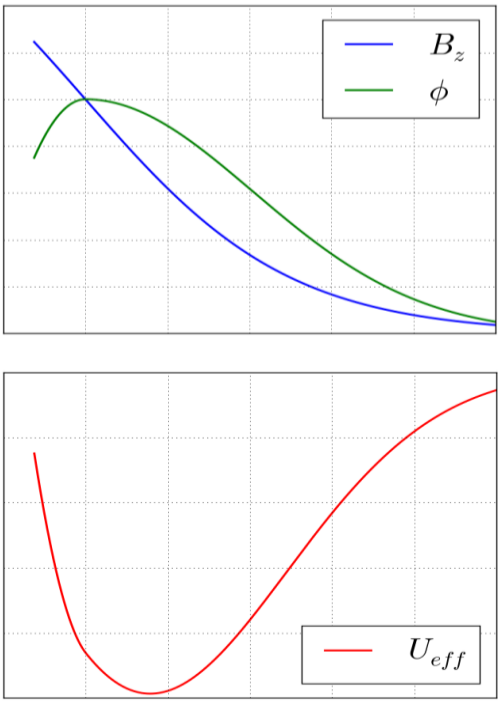

Figure 6. Typical profiles plotted against z (as defined on Figure 1). The plotted interval in z is typically 20cm. Top: axial component of the imposed magnetic field and typical electric potential as measured by LIF experiments[12]. Bottom: resulting "potential energy" for the guiding center of electrons for their motion along z

2. Energy distribution function

A typical energy distribution function is presented on Figure 8. It is measured in front of the thruster at the end near the wall of the tank, about 3m from the thruster. The mean ion energy is calculated to be 151eV and the most probable energy is between 155 and 170 eV. The distribution is not a symmetric beam but rather exhibits a gentler slope on the low energy side of the

maximum than on the high energy side. This low energy spread of the distribution is interpreted as a spread in ionization along the z axis. The energy of ions is dependent of the value of the electrostatic potential at the location where they are created. The shape of the distribution therefore indicates that substantial ionization is taking place away from the location of the maximum of the plasma potential and even outside of the material structure of the thruster (i.e. in the magnetic nozzle).

This measurement is made on the axis of symmetry of the thruster with the Hiden ion analyzer and measurements with the gridded Faraday probe show that the most probable ion energy is constant over angular position.

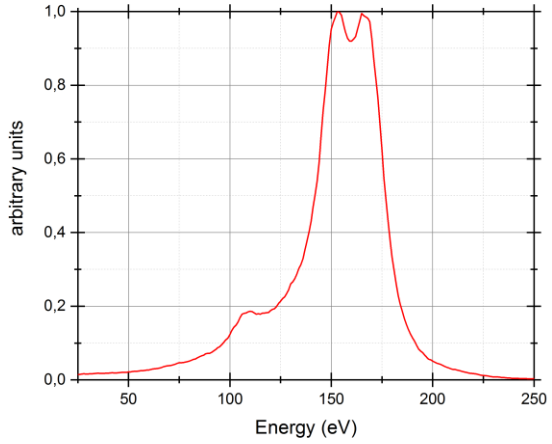

Figure 8. Typical ion energy distribution function for the coaxial ECRA thruster run at 1sccm Xe and 25W

3. *Ion current*

A typical ion current density profile is shown on Figure 7. It is strongly dependent with the imposed magnetic field indicating the critical effect of the magnetic field on the plasma expanding outside of the material structure of the thruster. In this case it is a quite centered profile providing a divergence efficiency above 0.75.

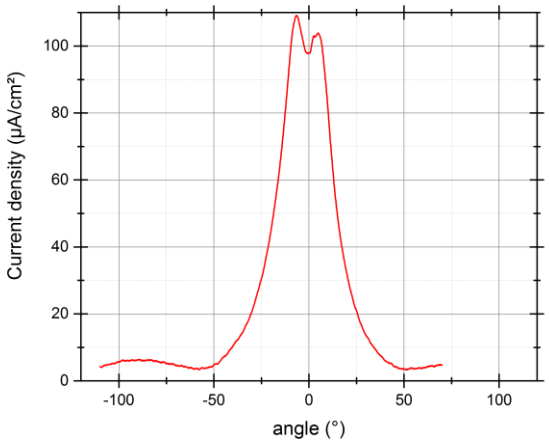

Figure 7. Typical ion current density angular profile for the coaxial ECRA thruster run at 1sccm Xe and 25W. The probe is placed 26.5cm from the exit plane of the thruster

Assuming (i) axis-symmetry of the jet, (ii) radial ion current, and (iii) detachment from the magnetic nozzle at the location of the measurement, the total ion current J_{tot} and thrust T can be estimated from the angular profile of the ion current density and from the mean ion velocity

$$J_{tot} = \pi D^2 \int_{-\pi/2}^{+\pi/2} J(\varphi)|\sin(\varphi)|d\varphi$$

$$T = \pi D^2 \frac{M}{e} \int_{-\pi/2}^{+\pi/2} v(\varphi)\, J(\varphi)\, |\sin(\varphi)|\cos(\varphi)\, d\varphi$$

where M is the ion mass, e is the elementary charge, D is the distance between the probe and the center of rotation of the arm that is moving the probe, φ is the angle of rotation of the probe defined to be 0 when the probe is on the axis of symmetry of the thruster, J and v are respectively the density of ion current and the ion velocity.

It is found that this integration consistently overestimates thrust with respect to what is measured by the thrust balance by a 20% to 80% factor dependent on the thruster configuration. In the case of the profile presented on Figure 7 the estimation yields 820 µN whereas 460µN is measured on the thrust balance. Such a discrepancy is beyond the customary 10 to 20 % error observed between direct thrust measurement and estimation with electrostatic probes on other type of thrusters.

It could be that one of the above mentioned assumption is not satisfied. Assumption (i) is verified, since the axis symmetry of the plume has been checked in the past. For assumption (ii), an experiment to check the direction of the flow of ions at the location of the measurements is among the top priorities. For assumption (iii), detachment is difficult to assess. Experiments have shown that for angles below 40° that the measured ion current profile at 26.5 cm is proportional to that taken at 58cm[14]. The size of the tank does not allow to perform this kind of experiment up to 90° whereas it seems a reasonable guess that a faulty measurement of the total current may come from the edges

rather than from the center of the angular distribution. Although interesting this result is not conclusive neither on the verification of assumption (ii) nor on (iii).

Perturbation of the plasma by the electrostatic probe could also result in overestimation of the ion current. The probe intercepts magnetic field lines that come out from the thruster. By imposing a highly negative bias voltage the probe sends back to the thruster electrons that would have, in the absence of the probe, sufficient energy to escape from the effective potential energy well. Since electrons are to a certain extent bound to magnetic field lines it results in the perturbation of all the magnetic field tube intercepted by the probe. This perturbation is likely to increase plasma density in the considered magnetic field tube, resulting in a higher ion current density measurement.

Using the integrated quantities J_{tot} and T as well as the mean ion energy, it is possible to estimate the efficiency of the thruster. It seems relevant to the analysis to break down the total efficiency into three multiplying factors that are the mass utilization efficiency, the power efficiency and the divergence efficiency. The mass utilization efficiency is the ratio of the ion mass flow rate extracted from the thruster to the input gas mass flow rate.

$$\eta_m = \frac{M}{e}\frac{J_{tot}}{\dot{m}_g}$$

The power efficiency is the ratio of the ion kinetic power exiting the thruster to the microwave input power P_{MW}.

$$\eta_E = \frac{M}{e}\frac{J_{tot}\, v^2}{2\, P_{MW}}$$

The divergence efficiency is the ratio of the effective thrust to what it would be if all the current were on the axis.

$$\eta_D = \frac{e}{M}\frac{T}{J_{tot}\, v}$$

Following these definitions, the total efficiency is

$$\eta_{tot} = \eta_m\, \eta_E\, {\eta_D}^2 = \frac{T^2}{2\, \dot{m}_g\, P_{MW}}$$

III. Measurements on the waveguide coupled thruster

Along with the waveguide coupled thruster a version of the coaxial coupled thruster was specifically designed to facilitate comparison. The waveguide and coaxial thrusters thereafter compared are identical except for the use waveguide or coaxial coupling structures and the material of the "backplate", imposed by the type of coupling. In particular, the magnetic field, the gas injection, and the geometry of the surfaces in direct contact with the plasma are the same.

The waveguide thruster ignites easily on the condition that a puff of gas is provided at start up. After about 90 minutes at 1sccm Xe and 20W of microwave power deposited in the plasma, the thruster reaches its temperature equilibrium around 110°C. The thruster frequency of the microwave power is empirically tuned to 2.25 GHz in order to minimize reflected power. The pressure in the test chamber is around 6.10^{-6} mbar when the thruster is operating

Figure 9. Front view of the waveguide coupled ECRA thruster in operation at 1sccm and around 20W. From this view angle only one of the six injection holes is clearly visible

at this set point. A picture of the thruster in operation is visible on Figure 9.

Figure 10 displays the thrust obtained by thrust balance measurement for several set points of mass flow rate and input power. As expected the thrust is increasing monotonically with mass flow rate and with power. A saturation is clearly visible for mass flow rate and the highest total efficiency of 3.8% is reached at 1.5 sccm and 16W. Thrusts are about 20% lower to that obtained with the coaxial coupled thruster.

The limitation in output power of the generator and the large amount of power reflected by the thruster (about 70% as compared to less than 5% with the coaxial thruster) prevented the exploration of higher powers. The high level of reflected power is an issue insofar that it increases the uncertainty of the input power measurement but is not a major issue for the development of the thruster since matching could be improved through a tuning of the microwave circuit or an increase in the size of the thruster. Experiments with a thruster the size of an RG-48 waveguide demonstrated only 10 to 20 % of reflected power (see section I).

Figure 11 displays the angular ion current density profile measured at several input power. The three curves are close to one another for angles above 40° whereas the difference in input power is much more visible in the central area where increase in power is clearly correlated with increase in ion current density.

The profiles are also plotted for several mass flow rates on Figure 12. The total current, thrust and efficiencies are calculated from electrostatic probe measurement from the angular ion current density profiles of Figure 12. These calculations are subject to error as described in section II.C.3. They are however presented on Table 1 along with the total efficiency from thrust balance measurements. Contrary to what could be expected the current density in front of the thruster (at 0°) is not monotonically increasing with mass flow rates. Neither is the total integrated current. Besides, the total integrated current is higher for the waveguide thruster than for the coaxial thruster at similar set points. The angular current density however is significantly more spread for the waveguide thruster resulting in a lower divergence efficiency. This could be explained by the shape of the propagating electromagnetic solutions in each coupling structure. The TE11 mode inserted in the waveguide is much more spatially homogeneous than the TEM mode inserted in the coaxial, which scales as the inverse of the radius of the location. An intense field in the center could induce a higher plasma density in the center which is then transported with little diffusion along the magnetic field lines to the plume of the thruster creating this peaked angular profile.

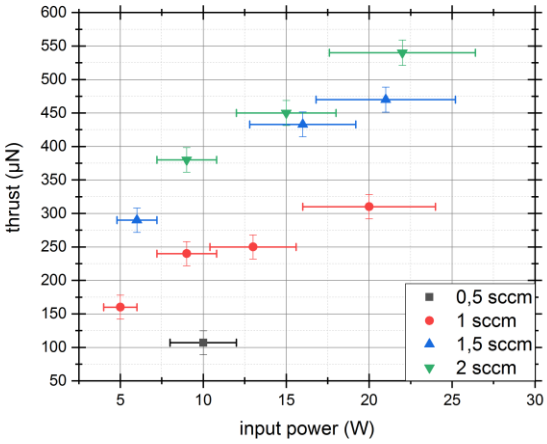

Figure 10. Thrust obtained from thrust balance measurement of the waveguide coupled thruster. It is plotted against the power deposited in the plasma for several mass flow rates of Xe. For reference, the coaxial coupled thruster produces 400µN of thrust at 1sccm and 24 W.

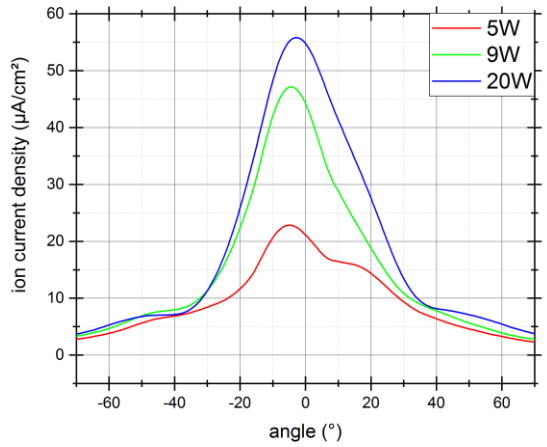

Figure 11. Ion current density angular profile measured at 26.5cm from the exit plane of the thruster with 1sccm Xe. Waveguide coupled thruster.

Besides, it is observed that the shape of the profiles depends on the mass flow rate contrary to the coaxial coupled thruster for which the profiles at different set-points are proportional (i.e. can be superposed by applying a multiplying factor on the y axis)[14].

Both thrusters exhibit quite similar energy distribution functions of the ions except around the maximum of the curves where the waveguide thruster profile is more sharply peaked (Figure 13). Both have quite a soft slope on the left side of the maximum interpreted as an image of ionization along the z axis (see section II.C.2). The mean energy

for the waveguide thruster is around 60 eV whereas it is around 150 eV for the coaxial thruster. This large discrepancy may be related to the same cause that is proposed to interpret the discrepancy in current. A locally more intense field existing in the center of the coaxial thruster could provide the high energy electrons which are necessary to build up a higher accelerating potential whereas the rather homogeneous field of the waveguide results in a high density of lower energy electrons.

Ion energies for several set points are presented on Figure 14 against input energy in electron volts of deposited microwave power per injected atom of neutral gas. The set of data taken from coaxial thrusters exhibits a linear increase in energy with a slope that is higher than that sketched by the cloud of data points from the waveguide thrusters. This plot suggests an intrinsic difference between waveguide coupled and coaxial coupled thrusters. Interpretation of this data should however be tempered by the fact that the background pressure has certainly lowered the ion energies measured by Sercel (1993) who reports a background pressure of 6.10^{-5} mbar. The experiment of Crimi (1967) on the other hand was reportedly run at a background pressure of 5.10^{-6} achieved with an oil diffusion pump.

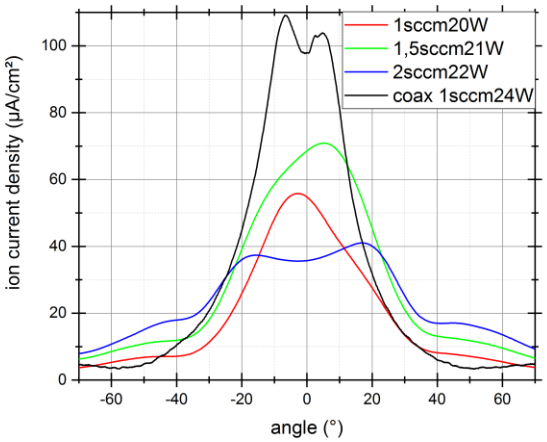

Figure 12. Ion current density angular profile measured at 26.5cm from the exit plane of the thruster with 1sccm Xe. Colored curves are measured for a waveguide coupled thruster and black curve is for coaxial coupled thruster.

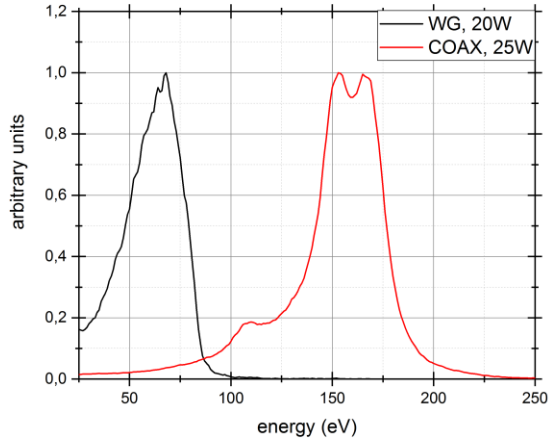

Figure 13. Ion energy distribution function for a waveguide coupled thruster and coaxial coupled thruster at 1sccm. Measured on the axis of symmetry of the thruster with Hiden ion analyzer

IV. Conclusion

The waveguide coupled thruster presented in this article is able to sustain a permanent regime and has been tested for several hours. A thrust of 430 µN at 1.5sccm and 16W of input power is measured with a thrust balance resulting in 3.8% of total efficiency. The comparison with a coaxial coupled thruster in an almost identical configuration showed that significantly more current is extracted from the waveguide thruster. It exhibits a less peaked ion current density profile whose shape is dependent on the set point. The ion

	$J_{tot}\ (mA)$	$T\ (\mu N)$	$E_i\ (eV)$	η_m	η_E	η_D	η_{tot}	η^*_{tot}
WG, 1sccm, 20W	68	390	60	0.93	0.20	0.44	0.04	0.02
WG, 1.5sccm, 21W	94	530	50	0.85	0.22	0.48	0.04	0.03
WG, 2sccm, 22W	84	500	40	0.57	0.15	0.57	0.03	0.03
COAX, 1sccm, 24W	54	820	150	0.74	0.34	0.75	0.14	0.03
COAX, different magnetic field and injection, at JLU Jumbo facility, 1sccm, 24W								0.14

Table 1. Energy is measured with the Hidden ion analyzer. Total integrated current, thrust, energy, mass utilization efficiency, power efficiency, divergence efficiency, and total efficiency are calculated from the electrostatic probe data presented on Figure 12. The total efficiency η^*_{tot} is calculated from thrust balance measurement.

energy distribution function follows the same shape on both thrusters but mean ion energy is much lower for the waveguide thruster. The discrepancy in energy between waveguide and coaxial coupling can be observed with other thruster configurations from the literature, suggesting that the ion energy it is an intrinsic feature of the type of coupling.

It is proposed that the discrepancies in ion current and ion energy could be explained qualitatively by the shapes of the propagating vacuum electromagnetic eigen modes of the respective coupling structure. However this explanation is insufficient in the presence of plasma. Self-consistent electromagnetic simulation would be extremely interesting to shed light on this matter.

If the results obtained here were consolidated by further studies, waveguide coupling would be an interesting avenue of investigation for the ECRA thruster.

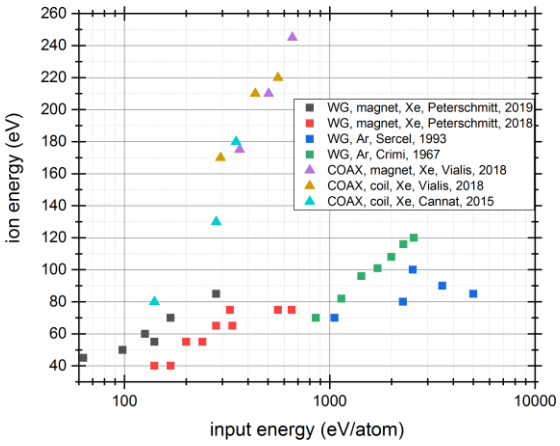

Figure 14. Ion energy plotted against input energy in eV per injected atom of neutral gas. Black data points are originally presented in this article. Colored points are from the litterature[8,9,11,14,15].

Acknowledgments

The authors thank Kristof Holste from JLU for organizing the test campaign from which results Figure 1 is extracted, and Jana Zorn from JLU for the design and operation of the thruster shown in Figure 5.

References

1. Wekerle, T. *et al.* Status and Trends of Smallsats and Their Launch Vehicles — An Up-to-date Review. *J. Aerosp. Technol. Manag.* **9**, 269–286 (2017).
2. Packan, D. *et al.* The "MINOTOR" H2020 project for ECR thruster development. in *35th International Electric Propulsion Conference, No. IEPC-2017-547, Electric Rocket Propulsion Society, Fairview Park, OH* (2017).
3. Cannat, F. *et al.* Optimization of a coaxial electron cyclotron resonance plasma thruster with an analytical model. *Phys. Plasmas* **22**, 053503 (2015).
4. Vialis, T., Jarrige, J., Aanesland, A. & Packan, D. Direct Thrust Measurement of an Electron Cyclotron Resonance Plasma Thruster. *J. Propuls. Power* **34**, 1323–1333 (2018).
5. Elias, P.-Q. Advances in the kinetic simulation of the microwave absorption in an ECR thruster. in (IEPC-2017-361, 2017).
6. Gibbons, E. F. & Miller, D. B. Experiments with an electron cyclotron resonance plasma accelerator. *AIAA J.* **2**, 35–41 (1964).
7. Crimi, G. F. E. *Microwave Driven Magnetic Plasma Accelerator Studies (CYCLOPS)*. (1967).
8. Crimi, G. F. Investigation of a Microwave Generated Plasma in a Non-Uniform Magnetic Field . (University of Pennsylvania, 1967).

9. Sercel, J. C. An experimental and theoretical study of the ECR plasma engine. (California Institute of Technology, 1993).
10. Vialis, T., Jarrige, J. & Packan, D. Geometry optimization and effect of gas propellant in an electron cyclotron resonance plasma thruster. in *Proc. 35th Int. Electr. Propuls. Conf* 1–12 (2017).
11. S. Peterschmitt, D. Packan, J. Jarrige. Waveguide microwave coupling to a magnetic nozzle ECR thruster. in (2018).
12. Jarrige, J., Correyero Plaza, S., Elias, P.-Q. & Packan, D. Investigation on the ion velocity distribution in the magnetic nozzle of an ECR plasma thruster using LIF measurements. in (2017).
13. Simon Peterschmitt, Jean C. Porto, Paul-Quentin Elias, Denis Packan. A diffusion model in velocity space to describe the electron dynamics in an ECR plasma thruster with magnetic nozzle. in (2019).
14. T. Vialis. Développement d'un propulseur plasma à résonance cyclotron électronique pour les satellites. (2018).
15. Cannat, F. Caractérisation et modélisation d'un propulseur plasma à résonance cyclotronique des électrons. (Ecole doctorale de l'Ecole Polytechnique, 2015).